Lu *et al. Journal of Translational Medicine* (2025) 23:1421
https://doi.org/10.1186/s12967-025-07401-6

Journal of Translational Medicine

RESEARCH Open Access

Intranasally administered muse cells attenuate neurodegeneration in Parkinson's disease

Zhe Lu[1†], Shifeng Ren[1†], Bingjie Wang[1†], Liwei Shao[1], Yajun Zhang[1], Haomeng Wu[1], Xiaodong Mu[1*] and Zhihui Wang[1*]

Abstract

Background Parkinson's disease is a neurodegenerative disorder primarily caused by the degeneration and death of dopaminergic neurons in the substantia nigra. Multilineage differentiating stress enduring (Muse) cells are a novel type of stem cells discovered in recent years, exhibiting superior tissue regenerative capabilities compared to regular mesenchymal stem cells, including multi-lineage differentiation potential, stress tolerance, homing ability, in situ differentiation capacity, and non-tumorigenic properties. Here we investigated the effect and mechanism of muse cell in crossing blood-brain barrier (BBB), and improving Parkinson's disease-related phenotypes.

Methods We used transwell to construct an in vitro blood-brain barrier model and treated it with muse cells and non-muse cells to observe the changes. We also used fluorescence confocal microscopy to examine the immunofluorescence sections of the hippocampal region of mice to explore changes before and after the treatment.

Results With an in vitro blood-brain barrier model, muse cells were found to have increased capacity to cross blood-brain barrier when tumor necrosis factor-alpha (TNF-α) was applied to mouse neuronal cells. Further experiments revealed that TNF-α increased the expression of sphingosine-1-phosphate (S1P) in neuronal cells, and high concentrations of S1P was able to activate the S1PR2-Rho pathway, leading to reduced expression of β-Catenin and increased BBB permeability. Thus, this indicate that muse cells possess an S1P-S1PR2 homing mechanism, enabling them to cross BBB. When muse cells were transplanted into A53T mice (a Parkinson's disease model) through nasal administration, muse cells exhibited stronger brain-homing ability compared to non-muse cells, by responding to specific signals released from damaged brain regions Additionally, muse cells have the potential to precisely differentiate into cells possessing key characteristics of dopaminergic neurons— tyrosine hydroxylase (TH) positive cells, which is also a defining feature of functional dopaminergic neurons. This observed increase in TH + cells holds substantial significance in Parkinson's disease, as TH is the rate-limiting enzyme in dopamine synthesis and is essential for restoring dopaminergic function and improving motor symptoms. While mesenchymal stem cells (MSCs) or induced pluripotent stem cell (iPSC)-derived neurogenic cells have also been shown to generate TH + cells

†Zhe Lu, Shifeng Ren and Bingjie Wang contributed equally to this work.

*Correspondence:
Xiaodong Mu
muxiaodong@sdfmu.edu.cn
Zhihui Wang
wangzhihui@sdfmu.edu.cn

Full list of author information is available at the end of the article

in preclinical models, muse cells offer distinct advantages, including innate tropism toward damaged tissue, stable integration, and a lower risk of tumor formation. The ability of muse cells to efficiently migrate, differentiate into functional dopaminergic phenotypes, and contribute to neural repair underscores their therapeutic potential and highlights their relevance in modeling and treating Parkinson's disease.

Conclusions These findings suggest that Muse cells achieve homing through the S1P-S1PR2 mechanism and intranasal administration of muse cells was efficient in reaching to the brain, which may offer a novel therapeutic strategy for Parkinson's disease.

Introduction

Parkinson's disease (PD) is a chronic progressive neurological disorder primarily characterized by motor dysfunction. The hallmark pathological feature of PD is the degeneration of dopaminergic neuron s in the substantia nigra of the midbrain, leading to a significant decrease in dopamine levels, which in turn triggers a series of motor and non-motor symptoms [1]. Studies have shown that the abnormal increase in blood-brain barrier (BBB) permeability in Parkinson's patients may be closely related to various factors, including endothelial cell damage, astrocyte dysfunction, and pericyte loss [2–4].

Stem cell-based therapies have been extensively explored as potential treatments for neurodegenerative diseases, and commonly studied stem cell types have been embryonic stem cells (ESCs) [5], induced pluripotent stem cells (iPSCs) [6, 7], mesenchymal stem cells (MSCs) [8], and neural stem cells (NSCs) [9]. However, both ESCs and iPSCs carry the risk of tumor formation, and their safety in clinical applications has not been fully guaranteed [10–12]. Neural stem cells exhibit low survival rates in the host brain, potentially due to immune rejection, inflammatory environments, or insufficient nutritional support. On the other hand, mesenchymal stem cells, with their advantages of wide availability and non-tumorigenicity, are considered a potential source for stem cell therapy. However, MSCs also have certain limitations, such as weak differentiation capacity and short survival time in vivo [13, 14].

In 2010, Kuroda et al. first reported "multilineage-differentiating stress-enduring cells" (muse cells) [15]. Under prolonged trypsin digestion conditions, most bone marrow mesenchymal stem cells or dermal fibroblasts died, but a small number of cells survived. These cells specifically express SSEA-3, as well as pluripotency genes such as Oct3/4, Nanog, and Sox2, and can differentiate into cells of all three germ layers from a single cell. Compared to mesenchymal stem cells, muse cells exhibit superior capabilities, including trilineage differentiation potential, stress tolerance, homing ability, in situ differentiation capacity, and non-tumorigenicity, which have garnered increasing research interest and attention. In animal models and clinical studies of various neurological diseases, muse cells have demonstrated promising therapeutic effects [16, 17], indicating their significant potential for application in Parkinson's disease research. Muse cells can be isolated and purified using flow cytometry and immunomagnetic sorting techniques [18, 19]. Research has shown that muse cells possess unique homing abilities, enabling them to migrate to damaged tissue sites, spontaneously differentiate into cell types compatible with the local tissue, and promote tissue repair. These cells exhibit strong tolerance in harsh environments and can survive for extended periods. Notably, muse cells typically remain dormant under normal physiological conditions and are activated only upon tissue injury [15]. The study by Yamada Y et al. revealed the molecular mechanism underlying the homing ability of muse cells [20]. It was found that muse cells highly express S1PR2 (sphingosine-1-phosphate receptor 2), with significantly higher levels compared to non-muse cells. This may be a key factor limiting the homing ability of non-muse cells. In various disease models, including liver fibrosis, spinal cord injury, and myocardial infarction, muse cells consistently demonstrated superior homing capabilities compared to non-muse cells. Further research showed that silencing S1PR2 using siRNA or treating muse cells with the S1PR2-specific antagonist JTE-013 significantly inhibited their specific homing to injury sites [20].

Therefore, in this study, we examined the potential protective effect of muse cell on neuronal cells and neurodegenerative phenotypes of Parkinson's disease with the mice model, and verified whether S1P-S1PR2 axis play a role in mediating the homing ability of muse cell to brain tissues. This study provides the first evidence that muse cells exhibit efficient lesion-directed homing capability in a Parkinson's disease mouse model, leading to significant neurofunctional restoration. This discovery not only identifies an ideal cell candidate for cell therapy in Parkinson's disease and potentially other neurodegenerative diseases or tissue damages, with improved outcomes compared to conventional stem cells, but also reveals a unique "active targeting-in situ repair" mechanism, holding substantial value for theoretical advance and broad prospects for clinical translation.

Materials and methods

Cell source

Human Umbilical Cord Mesenchymal Stem Cells (MSCs) was purchased from Procells, China. The medium was

replaced to remove non-adherent cells, and the adherent MSCs were then cultured for 3 passages. To get muse cells from MSCs, MSCs were incubated with SSEA3 antibody for 60 min, and then incubated with immunomagnetic beads (Miltenyi Biotec, Cat No. 130-047-401) for 15 min. SSEA3-positive cells were sorted using a magnetic stand. The positivity rates of muse cell markers (SSEA3 and CD105) were detected by flow cytometry. The primary astrocytes, pericytes, HBMEC cells, and mouse neuronal cells were all purchased from Procells, China.

Human umbilical cord mesenchymal stem cell line (purchased from Wuhan Procell Life Science & Technology Co., Ltd.) was cultured using Mesenchymal Stem Cell Medium (Huayan Biotechnology, cat. no. RMZ112). This complete medium was supplemented with Mesenchymal Stem Cell Serum-Free Medium Supplement (cat. no. NC0106.S) and 1% (v/v) Penicillin-Streptomycin Solution (containing 100 U/mL penicillin, 100 μg/mL streptomycin, and 50 μg/mL gentamicin; Solarbio, cat. no. P1410). Astrocytes, pericytes, and HBMEC cells (purchased from Wuhan Procell Life Science & Technology Co., Ltd.) were cultured using basal medium (DMEM; Vivacell, cat. no. 11995065). This complete medium was supplemented with 10% (v/v) heat-inactivated fetal bovine serum (FBS; Gibco, cat. no. C3113) and 1% (v/v) Penicillin-Streptomycin-Gentamicin Solution (containing 100 U/mL penicillin, 100 μg/mL streptomycin, and 50 μg/mL gentamicin; Solarbio, cat. no. P1410). All cells were cultured in a humidified incubator at 37 °C with 5% CO_2.

Experimental animals

This study employed 10 C57BL/6CI mice (12 months, females) and 30 A53T homozygous transgenic mice (12 months, females). The mice were housed in an environment maintained at 26 ± 2 °C with a 12-hour light/dark cycle, and were provided with free access to food and water. Experiments were performed using isoflurane to anesthetize C57 mice by inhalation. Two to three minutes after the administration of the drug, the animals showed slowing of respiration and disappearance of the turning reflex, and entered the surgical anesthesia period. Intraoperative body temperature (37 ± 0.5 °C) was maintained by a heating pad, and oxygen saturation (≥ 95%) was continuously monitored. At the end of the experiment, the mice were euthanized via carbon dioxide inhalation. The experiment has been reported in line with the ARRIVE guidelines 2.0.

CCK-8 assay

The mouse neuronal cell suspension was seeded into a 96-well plate, with 100 μL added to each well. The 96-well plate was placed in a 37 °C, 5% CO_2 incubator to allow cell attachment. Different concentrations of TNF-α were added, and the cells were further cultured for a specified period. Then, 10 μL of CCK-8 (Beyotime Cat No: C0041) reagent was added to each well and gently mixed. The 96-well plate was returned to the incubator and incubated for 1–4 h, with periodic observation of color changes. The absorbance (OD value) of each well was measured at a wavelength of 450 nm using a microplate reader.

Establishment of an in vitro blood-brain barrier model

The underside of the Transwell inserts was coated with Poly-L-lysine solution (Beyotime, Cat No.: C0312) and placed in a 37 °C, 5% CO_2 incubator for 1 h. After 1 h, the Transwell inserts were removed from the incubator, and any residual Poly-L-lysine was washed off with sterile water. A 30 μL cell suspension of astrocytes (1×10^5 cells) and pericytes (2×10^4 cells) was carefully applied to the underside of the inserts. The bottom of the culture plate served as a "lid," and the plate was then returned to the incubator to allow cell attachment for 3 h. After this period, the Transwell inserts were inverted, and any excess medium was aspirated. A mixture of astrocyte and pericyte medium (1:1 ratio) was then added to both the apical and basolateral compartments. When the cell confluence reached 90%, the mixed medium of astrocytes and pericytes in the apical compartment was removed. Then, 100 μL of HBMEC cell suspension (1×10^5 cells) was added to the apical compartment of the Transwell insert. The medium was supplemented with endothelial cell medium to a final volume of 500 μL, and the culture plate was returned to the incubator (Fig. 2A). Subsequently, the blood-brain barrier model was treated with high-concentration S1P (10 μM), low-concentration S1P (10 nM), and high-concentration S1P (10 μM) combined with the S1PR2 antagonist (JTE-013) for intervention.

Transendothelial electrical resistance (TEER) measurement

TEER measurement (Beijing Jingong Hongtai Technology Co., Ltd.) is a critical method for evaluating cell barrier function and is commonly used to assess the integrity of cell models. The electrodes were cleaned with 70% ethanol, and the Transwell cell culture plate was removed from the incubator and allowed to equilibrate to room temperature. The TEER electrodes were inserted into the Transwell inserts, ensuring contact with the medium without touching the cell layer. The resistance values were recorded, typically expressed in $\Omega \cdot cm^2$. The resistance of a blank Transwell insert was measured and subtracted from the sample values. The TEER value was calculated using the formula: TEER = (measured value - blank value) × membrane area.

Transmigration assay of muse cells

After the blood-brain barrier model was established, different concentrations of S1P were added to the medium in the lower chamber. Subsequently, an equal number of muse cells and non-muse cells, which constituted the SSEA3-negative fraction remaining after the immunomagnetic sorting of human umbilical cord MSCs, were used for subsequent experiments., as well as muse cells and non-muse cells treated with JTE-013 (an S1PR2 antagonist), were added to the upper chamber (all cells were labeled with PKH-26). After 48 h of culture, the migration of muse cells and non-muse cells was observed using immunofluorescence.

Western blot

Protein samples were collected from cells (neuronal cells, HBMEC cells, astrocytes, and pericytes) and brain tissue samples from each group of mice. Total protein was extracted using lysis buffer (e.g., RIPA buffer). After centrifugation, the supernatant was collected, and protein concentration was determined using the BCA assay. Protein samples were mixed with loading buffer and boiled for 10 min. The samples were then loaded into the wells of a polyacrylamide gel for electrophoretic separation. The separated proteins were transferred from the gel to a PVDF or nitrocellulose membrane. The membrane was blocked with 5% skim milk solution and incubated at room temperature for 1 h. The membrane was then incubated with primary antibodies (Table 1) at 4 °C overnight. After incubation, the membrane was washed three times with TBST buffer, each for 5–10 min. The membrane was subsequently incubated with HRP-conjugated secondary antibodies at room temperature for 1 h. The membrane was washed again three times with TBST buffer, each for 5–10 min. Finally, the membrane was incubated with ECL chemiluminescence reagent, and signals were detected using an imaging system.

Table 1 Antibody reagents

Rat/IgM SSEA3 Monoclonal Antibody (MC-631)	MA1-020	thermo
CD105 (Endoglin) Monoclonal Antibody (SN6), PE	12-1057-42	thermo
Goat anti-Rat IgM (Heavy chain) Cross-Adsorbed Secondary Antibody, Alexa Fluor™ 488	A-21,212	thermo
RHOA Polyclonal antibody	10749-1-AP	Proteintech
TNF Alpha Monoclonal antibody	60291-1-Ig	Proteintech
Anti-S1P(ab140592)	ab140592	abcam
β-Catenin Monoclonal antibody	51067-2-AP	Proteintech
TH Polyclonal antibody	25859-1-AP	Proteintech
BDNF Polyclonal antibody	28205-1-AP	Proteintech
GDNF Polyclonal antibody	26179-1-AP	Proteintech
NeuN Polyclonal antibody	26975-1-AP	Proteintech
Beta Actin Polyclonal antibody	20536-1-AP	Proteintech
Alpha Tubulin Recombinant antibody	80762-1-RR	Proteintech

Small animal in vivo imaging

Animal grouping: the normal group used 12-month-old female C57/BL6 mice (Control), and the PBS group used 12-month-old female A53T mice. PKH-26-labeled muse cells, non-muse cells, and muse + J cells (1×10^6 cells) were injected through nasal administration [21]. After injection, the mice were housed for 48 h, then anesthetized, and the distribution of cells in the brain was observed using small animal in vivo imaging technology (After completing the small animal in vivo imaging, the mice were continued to be raised for 2 weeks, followed by behavioral experiments. After the behavioral experiments, the brain tissues of the mice were collected for subsequent experimental analysis) (Fig. 4A).

Immunofluorescence

Adherent cells were fixed with 4% paraformaldehyde for 15–20 min at room temperature. The samples were then permeabilized with 0.1% Triton X-100 for 5–10 min at room temperature. Blocking was performed using goat serum for 30 min at room temperature to reduce non-specific binding. Primary antibodies (Table 1) were added and incubated at 4 °C overnight. After incubation, the samples were washed three times with PBS, each for 5 min. Fluorescently labeled secondary antibodies and Phalloidin (for cytoskeleton staining) were added and incubated in the dark at room temperature for 1 h. The samples were washed again three times with PBS, each for 5 min. Nuclei were stained with DAPI for 5–10 min at room temperature. Slides were mounted using anti-fade mounting medium to prevent drying and fluorescence quenching. Images were captured using a fluorescence microscope.

RhoA activity assay

RhoA activity in cell lysates was measured using the G-LISA RhoA Activation Assay Kit (Cytoskeleton Inc., Denver, CO, USA, cat. no. BK121) according to the manufacturer's protocol. Briefly, both muse and non-muse cells treated with different concentrations of an S1PR2 antagonist were lysed in 80 µL of the kit's lysis buffer. The protein concentration of the lysates was determined using the Precision Red protein assay, and all samples were normalized to the same concentration. The normalized samples were then added to the microplate wells and incubated at 4 °C for 30 min, as directed by the manufacturer's instructions. Luminescence was measured using a microplate reader.

Tissue sectioning

Tissue Samples: Mouse brain tissues were fixed with 4% paraformaldehyde at 4 °C overnight. After fixation, the tissues were rinsed with PBS to remove residual fixative. The tissues were then immersed in 15%-30% sucrose solution (4 °C, several hours to overnight) to reduce ice crystal formation. The tissue blocks were embedded in OCT compound, ensuring complete coverage. Sectioning: The embedded tissue blocks were rapidly frozen in dry ice (-50 °C to -80 °C). The cryostat was pre-cooled to -20 °C, and the section thickness was adjusted (typically 8 μm). Thin sections were gently transferred to pre-cooled glass slides using a brush or forceps. The sections were then subjected to immunofluorescence or H&E staining.

H&E staining

Tissue sections were dewaxed in xylene and rehydrated through a graded alcohol series (from high to low concentration) to gradually return the sections to a hydrated state. The sections were immersed in hematoxylin solution for several minutes. After staining, the sections were rinsed with running water to remove excess dye. The sections were then dipped in a weak acidic solution for differentiation to remove excess hematoxylin. After differentiation, the sections were rinsed again with running water. The sections were immersed in a weak alkaline solution to turn the hematoxylin-stained areas blue. The sections were then stained with eosin for several minutes. After staining, the sections were rinsed with running water to remove excess dye. Dehydration was performed through a graded alcohol series (from low to high concentration), followed by clearing with xylene. Finally, the sections were mounted with neutral resin and covered with coverslips for microscopic observation.

Behavioral experiment

Pole Test: Prepare a vertical pole with a diameter of 10 mm and a length of 50–60 cm. A small platform can be set at the top of the pole for placing the mouse. Before the experiment, allow the mice to familiarize themselves with the pole-climbing environment by conducting 1–2 training sessions. Place the mouse head-up at the top of the pole. Record the time required for the mouse to turn from head-up to head-down (T-turn) and the total time needed to climb from the top to the bottom of the pole (T-total). Perform 3–5 trials per mouse, and calculate the average to reduce variability. Analyze the data by comparing the turn time and total descent time among groups to assess differences in motor function.

Wire Hang Test: Prepare a metal wire with a diameter of 3 mm, fixed at a height of 30–40 cm above the ground. Before the experiment, allow the mice to familiarize themselves with the test environment by conducting 1–2 training sessions. Gently place the mouse's forepaws on the metal wire or horizontal bar, then release to allow the mouse to hang. Start timing when the mouse begins to hang, and stop when it falls or grabs the wire with all four paws. Perform 3–5 trials per mouse, with at least 10 min between trials, and calculate the average to minimize errors. Analyze the data by comparing the hanging time among groups to evaluate differences in muscle strength and endurance (To prevent excessive fatigue in the mice, the maximum value was set at 300 s).

Data statistics

For cell culture experiments, the sample size was determined to be at least three independent biological repeats (biological replicates, $n = 3$), with each experiment including three technical replicates (i.e., three measurements per sample). Data are presented as means ± standard error of the mean (s.e.m.), unless otherwise noted. Histological scoring was analyzed by the Kruskal-Wallis and Steel-Dwass tests, with a 95% confidence interval., Other statistical tests included two-tailed Student's t-tests and one-way ANOVA. For consistency in comparisons, significance in all figures is denoted as follows: $*P < 0.05$, $**P < 0.01$.

Results

S1P expression is elevated in neuronal cells with TNF-α treatment

S1P-S1PR pathway was found to be greatly involved in promoting cell transmigration across the blood - brain barrier [20]. Here we firstly examined whether the increased level of pro-inflammatory signaling in neuronal cells, which is a key feature of Parkinson's disease, may promote the activation of S1P expression.

The CCK8 assay results demonstrated that low concentrations of TNF-α (10–50 ng/ml) significantly promoted the growth of mouse hippocampal neuronal cells, while high concentrations of TNF-α (200–500 ng/ml) significantly induced apoptosis in mouse neurons (Fig. 1A). Therefore, we applied a TNF-α concentration of 300 ng/ml for subsequent experiments, and western blot results showed that the expression of S1P and TNF-α in TNF-α-treated mouse neuronal cells was significantly higher than that in the control group (Fig. 1B).

S1P impacts the permeability and tight junction protein expression of the in vitro blood-brain barrier model

The blood-brain barrier model was constructed using co-culture of astrocytes, pericytes, and HBMEC cells, TEER (trans-endothelial electrical resistance) results demonstrated that H-S1P significantly increased the permeability of the blood-brain barrier (significantly lower than the control group on days 1–4) (Fig. 2A).

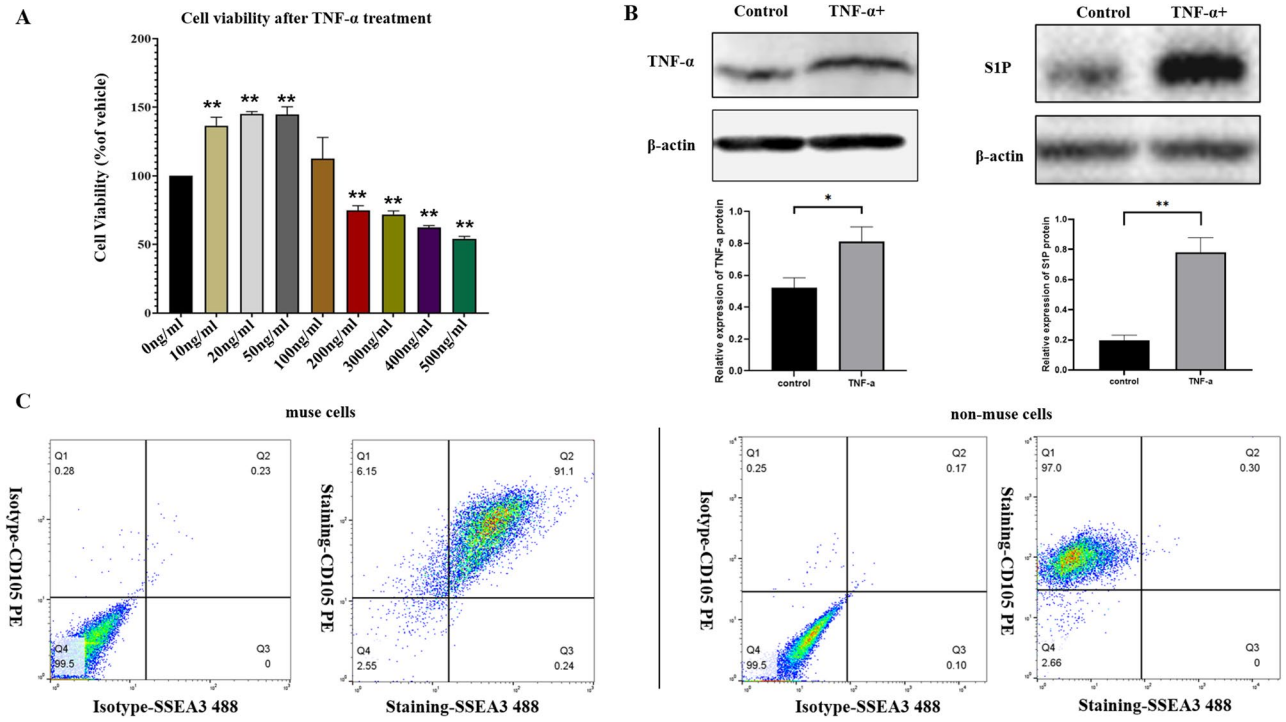

Fig. 1 S1P expression is elevated in neuronal cells with TNF-α treatment. **A**: CCK8 Assay Results: The CCK8 assay results showed that TNF-α at concentrations of 10–80 ng/ml stimulated the growth of mouse hippocampal neuronal cells, with a highly significant difference compared to the control group. In contrast, TNF-α at concentrations of 200–500 ng/ml induced apoptosis in mouse neurons, also showing a highly significant difference compared to the control group (Compared to the control group, $^{**}P < 0.01$) ($n = 6$). **B**: Western Blot Results: Western blot analysis revealed that the expression of TNF-α in mouse neuronal cells treated with 300 ng/ml TNF-α was significantly higher than that in the normal group. Additionally, the expression of S1P in TNF-α-treated mouse neuronal cells was significantly higher than that in the normal group (Compared to the control group, $^{*}P < 0.05$, $^{**}P < 0.01$) ($n = 3$). **C**: Muse and non-muse cells were isolated using the immunomagnetic sorting method, based on the expression level of SSEA3. Flow cytometry analysis revealed that the proportion of SSEA-3 and CD105 double-positive cells was 91.1% in muse cells, while it was only 0.3% in non-muse cells

Western blot analysis demonstrated that muse cells exhibited a more pronounced increase in S1PR2 expression compared to non-muse cells. The administration of the antagonist effectively reduced S1PR2 levels, confirming its efficacy (Fig. 2B).

Western blot results showed that, compared to the control group, and low concentration of S1P (L-S1P, 10 nM), high concentration of S1P (H-S1P, 10 μM) significantly upregulated the expression of RhoA and significantly downregulated the expression of β-Catenin in the blood-brain barrier model cells. Compared to the H-S1P group, the co-treatment of cells with H-S1P and S1PR2 antagonist (JTE-013) (group of H-S1P + J) failed to change the expression of RhoA and β-Catenin (Fig. 2C).

Immunofluorescence staining of the blood-brain barrier model showed high expression of β-Catenin in the control and L-S1P groups, with intact cell connections and well-preserved F-actin cytoskeleton structure as indicated by phalloidin staining. In the H-S1P group, β-Catenin expression was reduced, and both cell connections and cytoskeleton structure were disrupted. In the H-S1P + J group, cell connections and cytoskeleton structure were relatively intact (Fig. 2D).

The RhoA activity assay demonstrated that increasing concentrations of the S1PR2 antagonist progressively reduced RhoA activity in both muse and non-muse cells. Moreover, the muse cell group exhibited consistently higher RhoA activity compared to the non-Muse group across all concentrations tested (Fig. 2E).

Muse cell has improved trans-endothelial migration capacity than non-muse cells

Muse and non-muse cells were isolated using the immunomagnetic sorting method, based on the expression level of SSEA3. Flow cytometry analysis revealed that the proportion of SSEA-3 and CD105 double-positive cells was 91.1% in muse cells, while it was only 0.3% in non-muse cells (Fig. 1C).

The transwell assay was performed to compared the trans-endothelial migration capacity of muse cells and non-muse cells. Results demonstrated that, compared to non-muse cells, muse cells exhibited significantly higher trans-endothelial migration capacity in the blood-brain barrier model treated with high-concentration S1P, which was markedly reduced after adding JTE-013 (Fig. 3A).

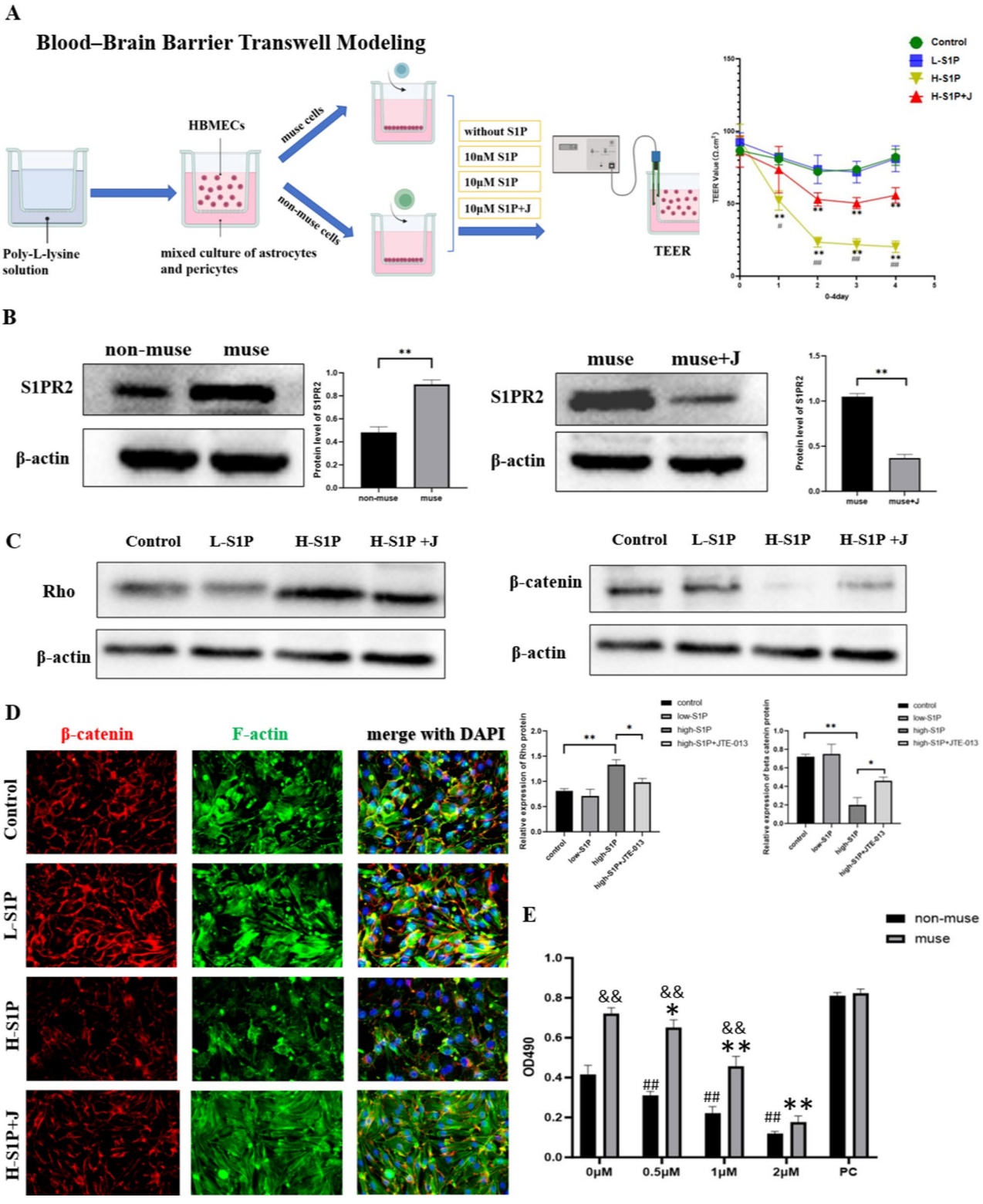

Fig. 2 (See legend on next page.)

(See figure on previous page.)

Fig. 2 S1P impacts the permeability and tight junction protein expression of the in vitro blood-brain barrier model. **A**: Establishment of an In **Vitro** Blood-Brain Barrier and Transmembrane Assay (Figure created with BioRender.com), First-generation astrocytes, pericytes, and HBMEC cells were co-culured in the upper chamber of the transwell (Astrocyte: HBMEC: Pericytes = 5:5:1). The permeability of the H-S1P group was significantly reduced compared to the control group on days 1–4; L-S1P had no effect on the BBB, and after adding the JTE-013 antagonist, permeability increased on day 1 compared to the H-S1P group and significantly increased on days 2–4 (Compared to the control group, $^{**}P < 0.01$, and compared to the high-concentration S1P group, $\#P < 0.05$, $\#\#P < 0.01$) ($n = 3$). **B**: Compared to non-muse cells, muse cell showed increased the expression of S1PR2. Compared to the muse group, the muse + J group showed reduced expression of S1PR2. (Compared to the control group, $^{**}P < 0.01$). **C**: Compared to the control group, L-S1P showed no significant difference in the expression of Rho and Beta-Catenin in the blood-brain barrier (BBB) model cells, while H-S1P significantly increased the expression of Rho and significantly decreased the expression of β-Catenin in the BBB model cells. Compared to the H-S1P group, the H-S1P + J group showed reduced expression of Rho and increased expression of β-Catenin in the BBB model cells. (Compared to the control group, $^{*}P < 0.05$, $^{**}P < 0.01$) ($n = 6$). **D**: (200× magnification) β-Catenin was highly expressed in the control group and the L-S1P group, with phalloidin staining showing intact cytoskeletons, while β-Catenin was lowly expressed in the H-S1P group, with disrupted cell connections and cytoskeletons; in the H-S1P + J group, cell connections and cytoskeletons were relatively intact ($n = 6$). **E**: Effects of varying concentrations of the S1PR2 antagonist on RhoA activity in muse and non-muse cells. (Compared to the 0μM muse group, $^{**}P < 0.01$, and compared to the 0μM non-muse group, $\#\#P < 0.01$ compared to the non-muse group, $\&\&P < 0.01$) ($n = 3$)

Also, in contrast to the low-concentration S1P group, the high-concentration S1P group induced cytoskeletal (microfilaments and microtubules) contraction in muse cells, resulting in cell shrinkage, while the degree of contraction was attenuated in the high-concentration S1P + J group. (Fig. 3B).

Muse cell reaches to brain tissue in Parkinson's mice model

Muse cells and non-muse cells labeled with fluorescent PKH-26 were transplanted into Parkinson's mice model (A53T mice) via intranasal administration. In vivo small animal imaging results showed that mice injected with non-muse cells showed significant aggregation in the lungs, with no fluorescence signal detected in the head. In contrast, mice injected with muse cells exhibited distinct fluorescence signals in the head region, while the signal intensity was reduced in those injected with muse + J cells (Fig. 4B).

Analysis of brain tissue sections revealed the presence of PKH-26-labeled muse cells in both the cerebral cortex and substantia nigra regions. In contrast, non-muse cells were almost undetectable in the cerebral cortex and substantia nigra regions (Fig. 4C-E).

Muse cell has protective effects on DA neurons

Compared to normal WT mice, A53T mice showed a significant reduction in tyrosine hydroxylase (TH) and neuron-specific nuclear protein (NeuN) staining in the substantia nigra pars compacta (SNc) region. However, A53T mice injected with muse cells displayed a higher number of TH-positive and NeuN-positive cells, and PKH26-labeled muse cells were detected in this region. In contrast, A53T mice injected with muse + J cells or non-muse cells exhibited relatively fewer TH-positive and NeuN-positive cells (Fig. 5A).

Western blot analysis revealed that S1P expression in the brain tissue of A53T mice (PBS group) was significantly increased compared with normal WT mice. In the group treated with muse cells, S1P expression was markedly reduced relative to both the PBS and non-muse groups, though it remained higher than that in normal WT mice. The expression of TNF-α in the brains of PBS group was significantly increased compared to normal WT mice. Compared to the PBS group, the TNF-α expression was significantly reduced in the muse cell-injected group. The non-muse cell and muse + J cell groups also showed reduced TNF-α expression, but the degree of reduction was less than that of muse cell group. Compared with normal WT mice, A53T mice (PBS group) exhibited significantly lower expression levels of BDNF and GDNF in the brain. Administration of muse cells significantly increased the expression of these two neurotrophic factors in A53T mice compared to the PBS group. However, the expression levels in the non-muse cell group and the muse + J group were lower than those in the Muse cell group (Fig. 5B).

H&E staining results showed that in the substantia nigra region of normal WT mice, the tissue structure was intact, and the morphology of cell nuclei was clear. In the substantia nigra region of A53T model mice (PBS group), significant neuronal loss was observed, with abnormal neuronal nuclear morphology and blurred nuclear boundaries. Compared to the non-muse group and the muse + J group, the muse group exhibited significantly reduced neuronal damage, and its histomorphological characteristics were closer to those of normal WT mice (Fig. 5C).

Muse cell improves the behavioral defects of Parkinson's disease mice model

The pole test results revealed that the climbing and turning times were significantly prolonged in Parkinson's model mice compared to normal WT mice. In contrast, Parkinson's model mice injected with muse cells exhibited a significant reduction in both climbing and turning times compared to the untreated Parkinson's model mice (Fig. 6A).

The suspension test results indicated a significant decrease in suspension time for Parkinson's model mice compared to normal WT mice. While mice with muse

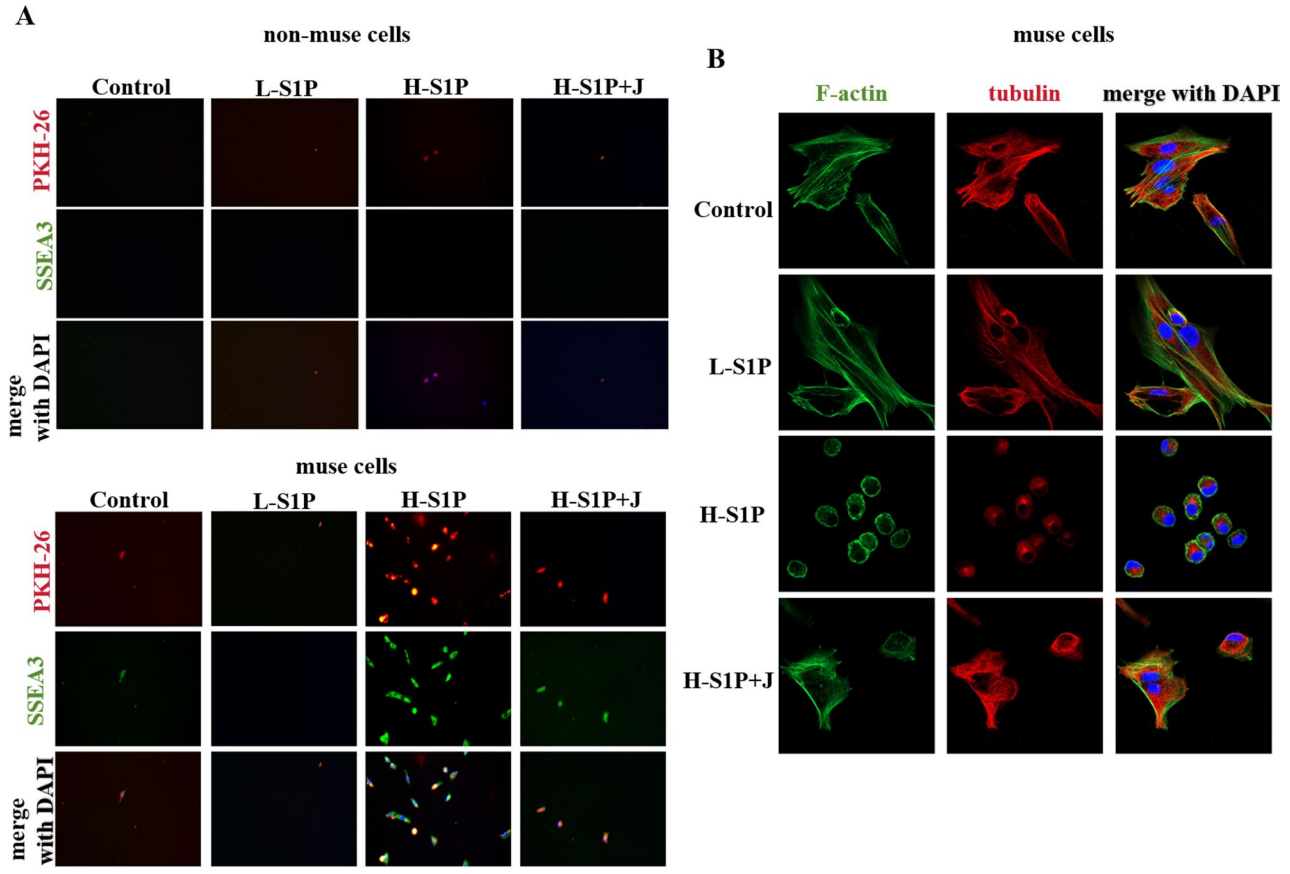

Fig. 3 Muse cell has improved transendothelial migration capacity than non-muse cells. **A**: (200×magnification) In the blood-brain barrier model, muse cells in the H-S1P group underwent transmembrane migration, while the migration of muse + J cells was reduced. Almost no cell migration was observed in the H-S1P group and the control group. Non-muse cells showed only a small amount of transmembrane migration in the H-S1P group of the blood-brain barrier model($n=6$). **B**: (630× magnification) Compared with the control group, the low-concentration S1P group showed no significant effect on the cytoskeleton of muse cells; the high-concentration S1P group induced cytoskeletal contraction in muse cells, while the degree of contraction was attenuated in the high-concentration S1P + J group ($n=6$)

cell injections demonstrated a significant increase in suspension time compared to their non-injected counterparts (Fig. 6B).

Discussion

Muse cells, a unique population of non-hematopoietic pluripotent stem cells, have been found to exhibit remarkable neuroprotective actions in the context of Parkinson's disease. The process involves the sphingosine – 1- phosphate (S1P) - S1P receptor 2 (S1PR2) - mediated transmigration across the blood-brain barrier (BBB). This intricate mechanism allows muse cells to reach the affected neural tissue in the brain. Once there, they can secrete various neurotrophic factors, which in turn help to protect dopaminergic neurons from degeneration, a hallmark of Parkinson's disease. By migrating through the blood - brain barrier following the S1P-S1PR2 pathway, muse cells hold great potential for developing novel therapeutic strategies against this neurodegenerative disorder.

The microstructure of the blood-brain barrier is composed of vascular endothelial cells, astrocytes, and pericytes [22]. The BBB separates the neuronal environment in the brain from peripheral blood, and its impairment is closely associated with inflammation and neurodegenerative diseases [23, 24]. Parkinson's disease (PD) is a common neurodegenerative disorder, and increasing evidence suggests that the function of the BBB is compromised in PD patients [3, 25]. A postmortem study of PD patients revealed that the integrity of the BBB in the striatum was disrupted, manifesting as erythrocyte extravasation, perivascular hemosiderin deposition, and leakage of various serum proteins. In rodent studies, it was found that treatment with the microbial neurotoxin BMAA significantly reduced BBB permeability in mice [25, 26]. Research has found that the nigrostriatal dopaminergic region and cerebrospinal fluid (including ventricular and lumbar CSF) of Parkinson's disease patients exhibit significantly elevated levels of pro-inflammatory cytokines such as tumor necrosis factor-α (TNF-α) are

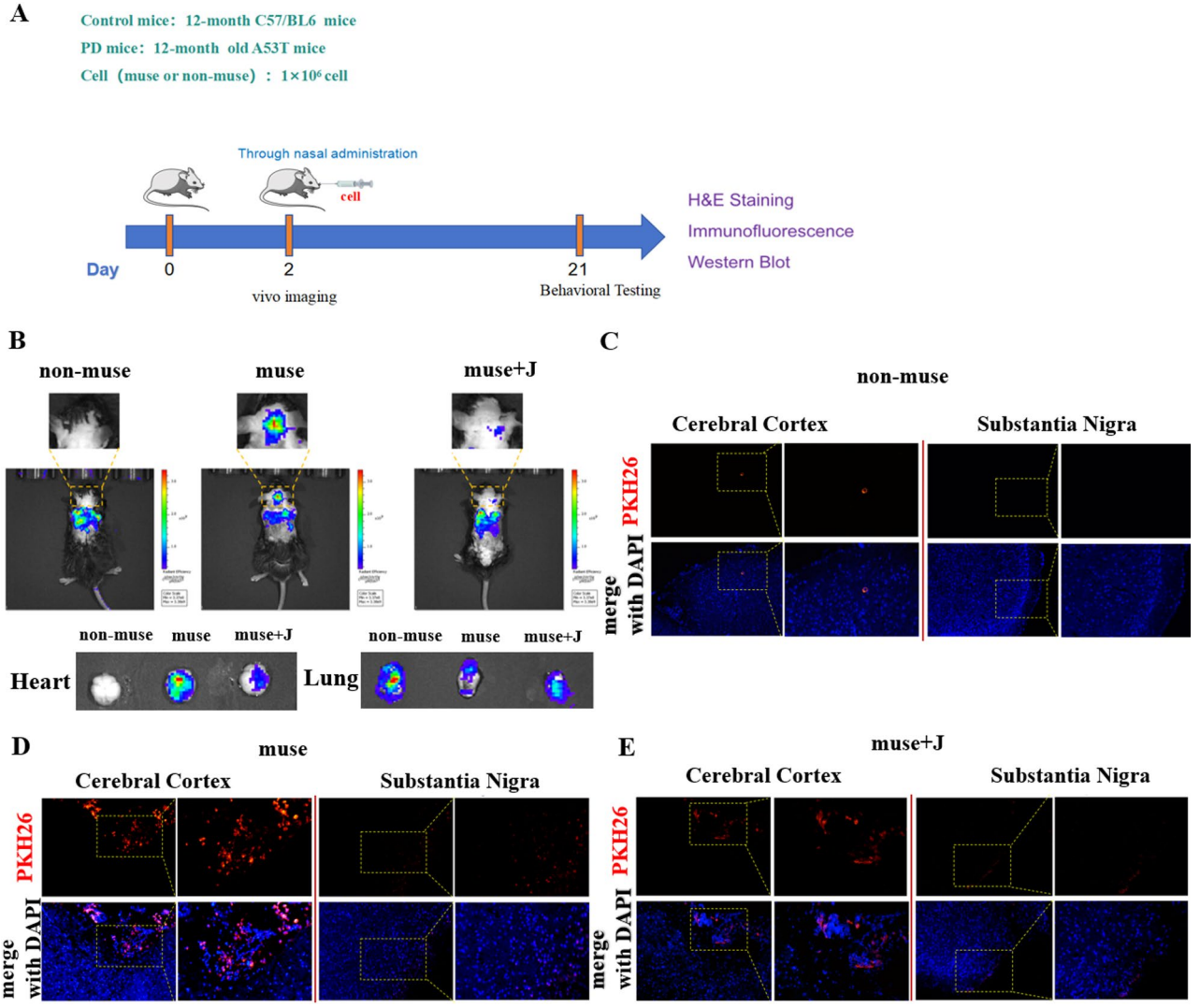

Fig. 4 Muse cell reaches to brain tissue in Parkinson's mice mode. **A**: Schematic diagram of in vivo experimental design. **B**: A53T mice injected with non-muse cells showed significant aggregation in the lungs, with no fluorescence signal detected in the head. In contrast, mice injected with muse cells exhibited distinct fluorescence signals in the head region, while the signal intensity was reduced in those injected with muse + J cells($n=3$). **C-E**: (200×magnification; 400×magnification) In brain tissue sections of mice, PKH-26-labeled muse cells and muse + J cells were observed in both the cerebral cortex and substantia nigra regions. The number of muse + J cells was relatively lower compared to muse cells, while non-muse cells were almost absent in the cerebral cortex and substantia nigra regions ($n=6$)

significantly elevated, while the levels of neurotrophic factors (e.g., BDNF, GDNF) are markedly reduced [26]. Correspondingly, a PD mouse model, pathological changes were observed, including increased expression of A1-type astrocytes (considered neurotoxic), loss of dopaminergic neurons in the substantia nigra, elevated blood-brain barrier (BBB) permeability, and reduced levels of neurotrophic factors [27]. This experimental study confirmed that, compared to the normal control group, the brains of PD model mice exhibited a characteristic pathological microenvironment: levels of the pro-inflammatory cytokine TNF-α were significantly elevated, while the expression of neurotrophic factors BDNF and GDNF was concurrently downregulated. This detrimental microenvironment ultimately led to a marked reduction in the number of cells positive for TH, a marker of dopaminergic neurons, and NeuN, a marker of mature neurons.

Sphingosine-1-phosphate (S1P) is a biologically active sphingolipid that plays a crucial role in the immune system. It is widely expressed throughout the body and is involved in the regulation of immune activation and cellular transport [28]. In addition to its immune functions, S1P also influences other critical cellular processes, including barrier integrity, angiogenesis, and cell proliferation, through its synthesis in platelets, red blood cells, vascular endothelial cells, and hepatocytes [29]. Growing evidence suggests that the S1P signaling

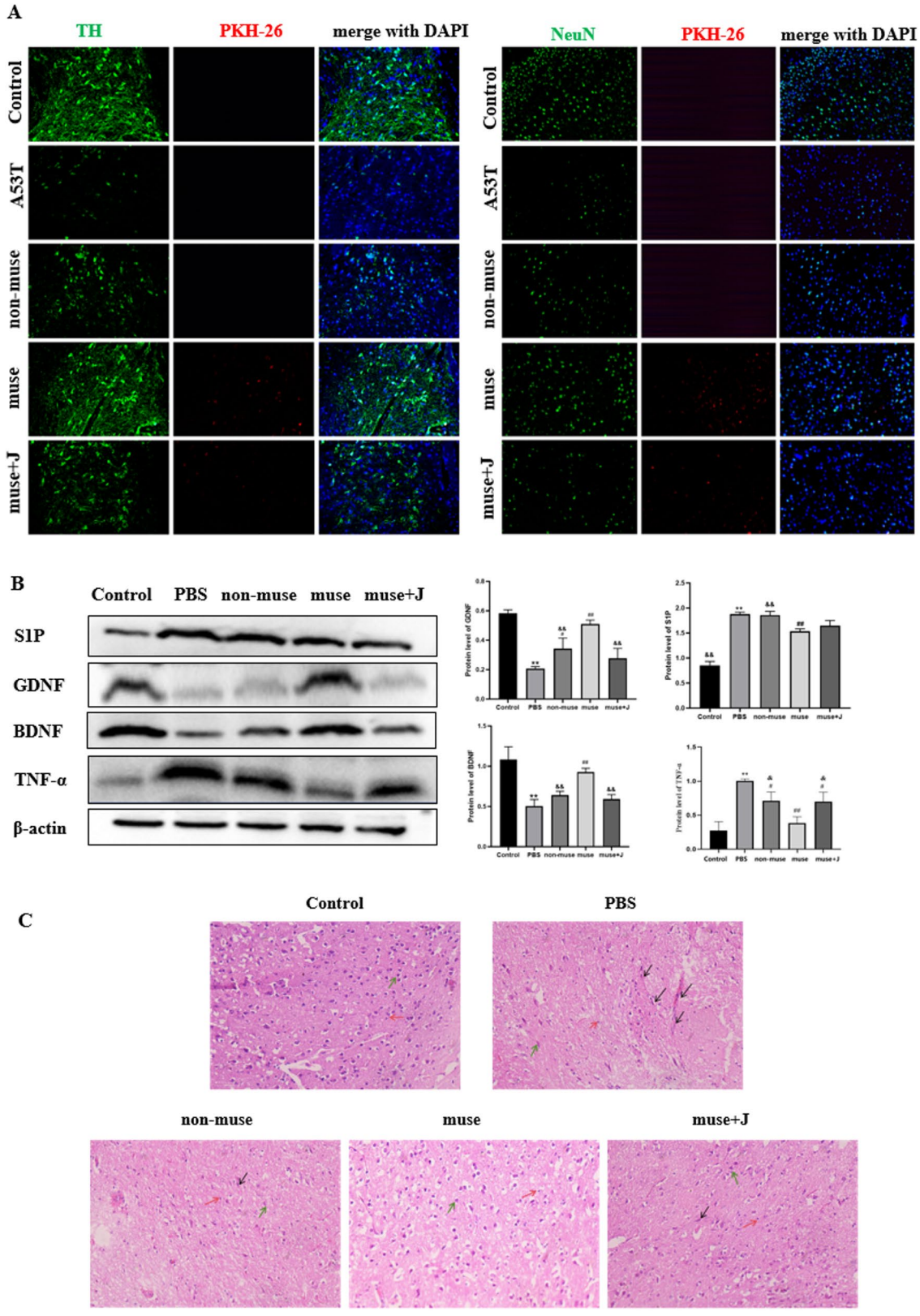

Fig. 5 (See legend on next page.)

(See figure on previous page.)

Fig. 5 Muse cell has protective effects on DA neurons. **A**: (200×magnification) Compared to normal WT mice, the PBS group showed reduced TH and NeuN staining in the SNc region. In contrast to the PBS group, the muse group exhibited a higher number of TH-positive cells and NeuN-positive cells, with PKH26-labeled muse cells present in the region. Compared to the muse group, the muse + J and non-muse groups displayed relatively fewer TH-positive cells($n=6$). **B**: S1P expression in the brain tissue of A53T mice (PBS group) was significantly increased compared with normal WT mice. In the group treated with muse cells, S1P expression was markedly reduced relative to both the PBS and non-muse groups, though it remained higher than that in normal WT mice. Western blot results indicated: TNF-α expression in the brains of the PBS group was significantly higher than in control. Compared to the PBS group, TNF-α expression was significantly reduced in the muse group, while the non-muse and muse + J groups also showed reduced TNF-α expression. TNF-α expression in the muse group was lower than in the non-muse and muse + J groups. Expression levels of BDNF and GDNF showed a marked decline in the PBS group. No significant change was seen with non-muse cell treatment, whereas the muse group displayed elevated expression. The expression remained unchanged in the muse + J group. (*Compared to the control group, **$P<0.01$, and compared to the PBS group, #$P<0.05$, ## $P<0.01$, & compared to the muse group, & $P<0.05$) ($n=3$). **C**: The H&E staining results (200× magnification) showed that in the substantia nigra region of normal WT mice, the tissue structure was normal, and the cell nuclei were clearly visible (red arrows indicate astrocytes, green arrows indicate neuronal cells). In contrast, the brains of PBS group mice exhibited significant neuronal loss, with abnormal neuronal nuclear morphology and blurred boundaries. The non-muse group and muse + J group showed similar conditions to the PBS group, but the degree of neuronal damage was reduced. In the muse group, the number of damaged neurons was significantly decreased, and the tissue characteristics were similar to those of normal WT mice. (red→astrocyte, green→neuronal cells, black→damaged neuronal cells) ($n=6$)

pathway regulates the structure and function of the BBB under pathophysiological conditions [30]. TNF-α, a pro-inflammatory factor, is implicated in various neurological disorders such as Alzheimer's disease (AD) and Parkinson's disease (PD) [31, 32]. TNF-α signaling stimulates the conversion of sphingosine to S1P by activating sphingosine kinase 1 (SK1), and elevated levels of TNF-α can mediate an increase in S1P content [33, 34]. A study based on data from stroke patients revealed that serum S1P levels significantly rise following cellular injury [35]. In this study, in vitro experiments demonstrated that high concentrations of TNF-α could induce neuronal apoptosis and upregulate S1P expression, suggesting that neuroinflammation and apoptosis in the brain may collectively promote S1P release. Furthermore, in vivo experiments showed increased expression of both TNF-α and S1P in the brains of A53T mice, further supporting the inference that inflammatory factors may stimulate S1P release.

S1P exerts its effects through five G protein-coupled receptors (S1PR1–5), among which S1PR1 and S1PR2 are selectively expressed in blood-brain barrier (BBB) cells and play significant roles in BBB function [36]. Research indicates that S1PR1 and S1PR2 maintain a balanced role in Rho GTPase signaling, collectively preserving the integrity of the BBB. Low levels of S1P bind to the S1PR1 receptor, activating the Rac signaling pathway, thereby enhancing BBB function [37–39]. Conversely, high levels of S1P bind to the S1PR2 receptor, leading to the breakdown of junctional proteins (such as β-Catenin) and promoting cytoskeletal contraction through RhoA signaling, thereby impairing BBB function [40, 41]. This study, by constructing an in vitro BBB model, found that high concentrations of S1P upregulate Rho expression and decrease β-Catenin expression, causing cytoskeletal changes in BBB model cells and increasing BBB permeability. However, when the S1PR2 antagonist (JTE-013) was added, Rho protein expression decreased, β-Catenin expression increased, and BBB permeability significantly reduced. In summary, alterations in the BBB in Parkinson's disease may be due to increased TNF-α expression, which in turn increases S1P secretion. S1P binding to the S1PR2 receptor promotes Rho signaling, leading to the loss of the junctional protein β-Catenin and cytoskeletal contraction, ultimately resulting in increased BBB permeability.

Our results further indicate that the S1P-S1PR2 axis is a unique mechanism that distinguishes the function of muse cells from non-muse cells [20]. Our experiments demonstrated that muse cells possess a significantly higher level of S1PR2 expression relative to their non-muse counterparts. When muse cells and non-muse cells were added to a blood-brain barrier (BBB) model with high concentrations of S1P, only muse cells exhibited significant migratory ability, accompanied by noticeable changes in their cytoskeleton, while the migration of non-muse cells was limited. Treatment of muse cells with the S1PR2 antagonist significantly inhibited their migration and reduced RhoA activity. Therefore, the mechanism by which muse cells can cross the blood-brain barrier may be related to the release of high concentrations of S1P in Parkinson's disease: high levels of S1P increase the permeability of the blood-brain barrier, and the high expression of S1PR2 receptors on muse cells enables them to respond to S1P released in the brain, thereby promoting their migration. Furthermore, the S1P-S1PR2 axis may promote the trans-endothelial migration of muse cells across the blood-brain barrier by modulating RHOA activity and consequently altering their cytoskeletal architecture.

Neurological disorders such as stroke, Alzheimer's disease, and Parkinson's disease are often associated with impaired neural regeneration, potentially leading to severe functional disabilities or even death. Studies have shown that muse cells can be induced to differentiate into neural stem cells, mature neurons, and astrocytes in vitro[42, 43], and can spontaneously undergo these differentiation processes in vivo. Increasing evidence suggests

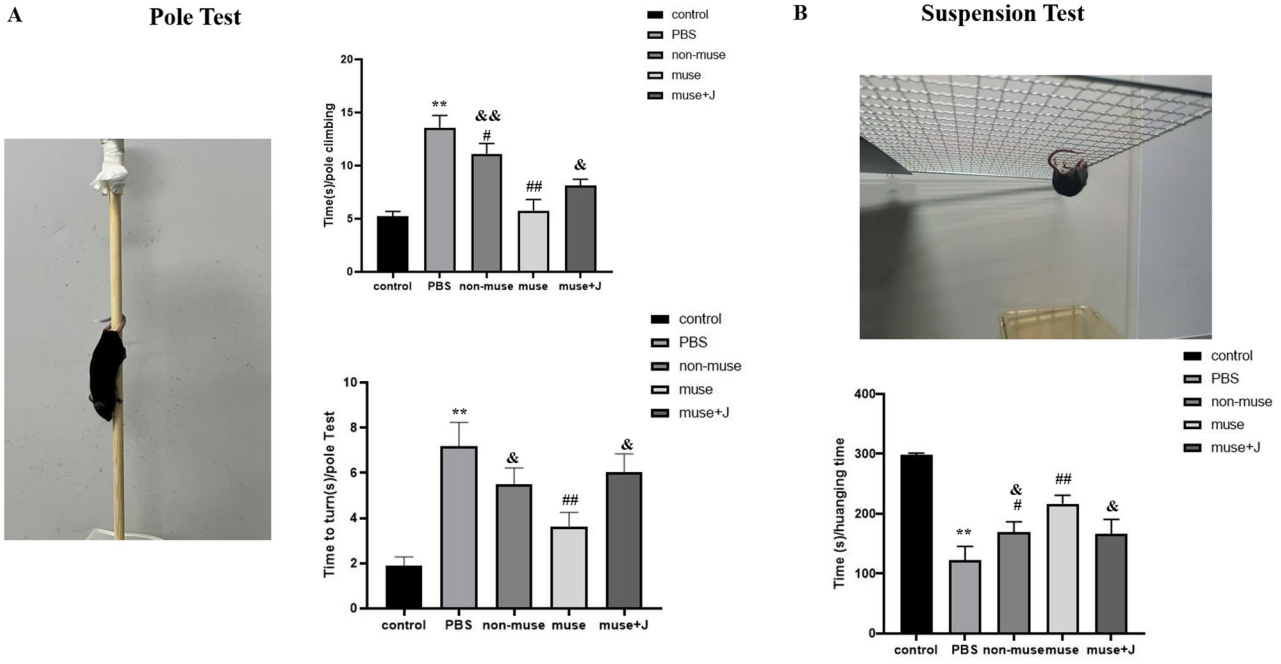

Fig. 6 Muse cell improves the behavioral defects of Parkinson's Disease mice model. **A**: The results of the pole test showed: Compared with control, the climbing and turning time of mice in the PBS group was significantly prolonged; compared with the PBS group, the climbing and turning time of the muse group was significantly shortened. Compared with the muse group, the climbing time of the non-muse group was significantly prolonged, and the turning time was prolonged; the climbing and turning time of the muse + J group was prolonged (*Compared to the control group, **$P < 0.01$, and compared to the PBS group, ## $P < 0.01$, & compared to the muse group, & $P < 0.05$, && $P < 0.01$) ($n = 6$). **B**: The results of the suspension test showed: compared with compared with control, the suspension time of mice in the PBS group was significantly shortened; compared with the PBS group, the suspension time of the muse group was significantly prolonged. Compared with the muse group, the suspension time of the non-muse group and the muse + J group was shortened (*Compared to the control group, **$P < 0.01$, and compared to the PBS group, #$P < 0.05$, ## $P < 0.01$, & compared to the muse group, & $P < 0.05$) ($n = 6$)

that muse cells can cross the BBB and exert therapeutic effects on various neurological disorders [44, 45]. In research on hypoxic-ischemic brain injury, 7-day-old rats underwent left carotid artery ligation and were exposed to 8% oxygen for 60 min. Seventy-two hours later, muse or non-muse cells (1×10^4 cells/rat) were intravenously injected [44]. The results showed that muse cells migrated to the injured brain region by the second week and differentiated into neuronal cells after six months, expressing neuronal markers such as NeuN and MAP-2, as well as oligodendrocyte markers like GST-pi. In contrast, non-muse cells primarily accumulated in the lungs, with no observed neural differentiation. Abe et al. further explored the application of muse cells in a lacunar cerebral infarction model [46], finding that a high dose (5 × 10^4 cells/rat) of muse cells significantly improved motor function in both acute (9 days post-injury) and chronic (30 days post-injury) phases. After 22 weeks, these cells were distributed around the infarct area and expressed neuronal markers. On the other hand, Studies have shown that intranasal administration of stem cells offers significant advantages over tail vein injection or other delivery routes: firstly, it achieves higher delivery efficiency to the central nervous system; secondly, it avoids first-pass metabolism, thereby enhancing the bioavailability of the drug; moreover, this method is non-invasive and easy to perform, allowing for repeated administration when necessary, which improves the flexibility of treatment; finally, since the therapeutic compounds are not exposed to other healthy organs, potential adverse effects can be minimized [47]. There are 2 primary hypotheses regarding the pathways by which drugs and cells reach the brain following intranasal delivery: the nose-to-brain nerve pathways (the olfactory pathway and the trigeminal nerve pathway) and the perivascular pathway. However, recent research has highlighted the significance of the perivascular pathway in cellular transport, demonstrating that neuroblasts derived from the olfactory bulb can migrate along vascular structures [48]. The underlying mechanism involves these cells utilizing blood vessels as a migratory scaffold/track, facilitating their movement through interactions with the extracellular matrix and the endfeet of perivascular astrocytes [49].

This study found that the substantia nigra region of the A53T transgenic mouse model exhibited reduced TH and NeuN staining intensity, significant neuronal loss and apoptosis, and accompanied by motor dysfunction. Compared to A53T mice injected with non-muse cells,

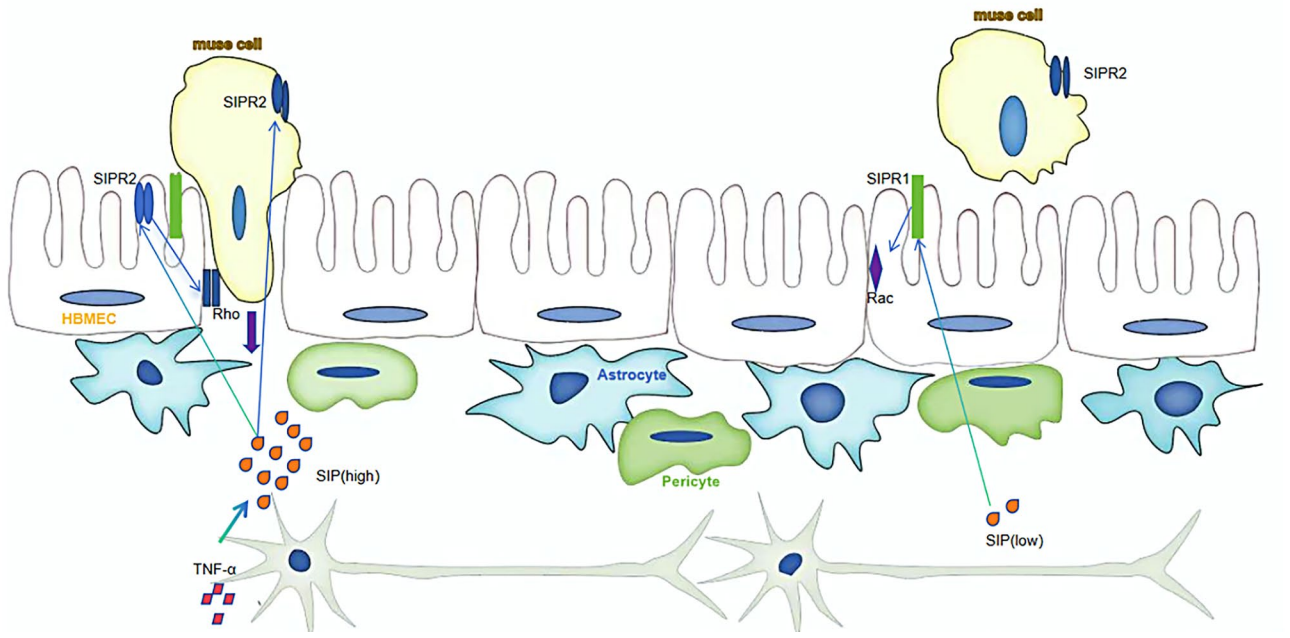

Fig. 7 Mechanism diagram of Muse cells crossing the blood-brain barrier

the group injected with muse cells showed a higher number of TH-positive cells, significantly reduced neuronal apoptosis, improved motor function, and the presence of PKH26-labeled muse cells in the region, along with alleviated neuroinflammation, increased expression of neurotrophic factors. However, in the A53T mouse group injected with S1PR2 antagonist-treated muse cells, the number of TH- and NeuN-positive cells was lower. Furthermore, the improvement in inflammatory response, the increase in neurotrophic factor expression, and the degree of motor function recovery were all inferior to those in the untreated muse cell group. Based on these results, we hypothesize that Parkinson's disease may trigger neuroinflammation and increase S1P concentration, activating the Rho signaling pathway, leading to disorganized cell arrangement and increased permeability of the blood-brain barrier. In this process, the S1P-S1PR2 system may mediate the migration of muse cells to the injury site, thereby exerting neuroprotective effects (Fig. 7).

Supplementary Information

The online version contains supplementary material available at https://doi.org/10.1186/s12967-025-07401-6.

Supplementary Material 1

Acknowledgements
This study was supported by research fundings from Shandong First medical University and Shandong Academy of Medical Science, and funding from Shandong Provincial Natural Science Foundation.

Author contributions
ZL, SR, XM and ZW performed literature search, study design, and paper writing; ZL, SR, BW and YZ performed experiments and data collection; ZL, SR and YZ performed data analysis. ZL, SR, YZ participated in article framework construction and critical revision. All authors read and approved the final manuscript.

Funding
Shandong Provincial Natural Science Foundation (ZR2022MC025).

Data availability
The data generated during the current study are available from the corresponding author on reasonable request.

Declarations

Ethics approval and consent to participate
All procedure of animal works had been approved by the research ethics committee of School of Pharmaceutical Science, Shandong First Medical University (Approval No. SYXK(LU) 2024 0019).

Consent for publication
All co-authors approve for the publication of the study.

Conflict of interest
Authors declare that they have no conflict of interest. This paper has not use AI-generated work in this manuscript.

Author details
[1]Shandong First Medical University & Shandong Academy of Medical Sciences, Jinan, Shandong, China

Received: 3 July 2025 / Accepted: 29 October 2025
Published online: 24 December 2025

References

1. Parkinson J. An essay on the shaking palsy. 1817. J Neuropsychiatry Clin Neurosci. 2002;14(2):223–36. discussion 2.

2. Lan G, Wang P, Chan RB, Liu Z, Yu Z, Liu X, et al. Astrocytic VEGFA: an essential mediator in blood-brain-barrier disruption in Parkinson's disease. Glia. 2022;70(2):337–53.
3. Gasca-Salas C, Fernandez-Rodriguez B, Pineda-Pardo JA, Rodriguez-Rojas R, Obeso I, Hernandez-Fernandez F, et al. Blood-brain barrier opening with focused ultrasound in Parkinson's disease dementia. Nat Commun. 2021;12(1):779.
4. Gasca-Salas C, Pineda-Pardo JA, Del Alamo M, Jimenez T, Trompeta C, Toltsis G, et al. Nigrostriatal blood-brain barrier opening in Parkinson's disease. J Neurol Neurosurg Psychiatry. 2024;95(11):1089–92.
5. Elabi OF, Pass R, Sormonta I, Nolbrant S, Drummond N, Kirkeby A, et al. Human embryonic stem cell-derived dopaminergic grafts alleviate L-DOPA induced dyskinesia. J Parkinsons Dis. 2022;12(6):1881–96.
6. Sonntag KC, Song B, Lee N, Jung JH, Cha Y, Leblanc P, et al. Pluripotent stem cell-based therapy for Parkinson's disease: current status and future prospects. Prog Neurobiol. 2018;168:1–20.
7. Li W, Chen S, Li JY. Human induced pluripotent stem cells in Parkinson's disease: A novel cell source of cell therapy and disease modeling. Prog Neurobiol. 2015;134:161–77.
8. Cerri S, Greco R, Levandis G, Ghezzi C, Mangione AS, Fuzzati-Armentero MT, et al. Intracarotid infusion of mesenchymal stem cells in an animal model of Parkinson's disease, focusing on cell distribution and neuroprotective and behavioral effects. Stem Cells Transl Med. 2015;4(9):1073–85.
9. Li F, Zhang A, Li M, Wang X, Wang X, Guan Y, et al. Induced neural stem cells from Macaca fascicularis show potential of dopaminergic neuron specification and efficacy in a mouse Parkinson's disease model. Acta Histochem. 2022;124(6):151927.
10. Lee AS, Tang C, Cao F, Xie X, van der Bogt K, Hwang A, et al. Effects of cell number on teratoma formation by human embryonic stem cells. Cell Cycle. 2009;8(16):2608–12.
11. Malik N, Rao MS. A review of the methods for human iPSC derivation. Methods Mol Biol. 2013;997:23–33.
12. Olgasi C, Cucci A, Follenzi A. iPSC-Derived liver organoids: A journey from drug screening, to disease modeling, arriving to regenerative medicine. Int J Mol Sci. 2020;21(17):6215.
13. Thomson JA, Itskovitz-Eldor J, Shapiro SS, Waknitz MA, Swiergiel JJ, Marshall VS, et al. Embryonic stem cell lines derived from human blastocysts. Science. 1998;282(5391):1145–7.
14. Bertolo A, Mehr M, Janner-Jametti T, Graumann U, Aebli N, Baur M, et al. An in vitro expansion score for tissue-engineering applications with human bone marrow-derived mesenchymal stem cells. J Tissue Eng Regen Med. 2016;10(2):149–61.
15. Kuroda Y, Kitada M, Wakao S, Nishikawa K, Tanimura Y, Makinoshima H, et al. Unique multipotent cells in adult human mesenchymal cell populations. Proc Natl Acad Sci U S A. 2010;107(19):8639–43.
16. Uchida H, Niizuma K, Kushida Y, Wakao S, Tominaga T, Borlongan CV, et al. Human muse cells reconstruct neuronal circuitry in subacute lacunar stroke model. Stroke. 2017;48(2):428–35.
17. Niizuma K, Osawa SI, Endo H, Izumi SI, Ataka K, Hirakawa A, et al. Randomized placebo-controlled trial of CL2020, an allogenic muse cell-based product, in subacute ischemic stroke. J Cereb Blood Flow Metab. 2023;43(12):2029–39.
18. Leng ZK, Gao ZC, He XJ, Zhao YJ, Sun LJ, Zhai JJ, et al. [Cultivation, screening, identification and transplantation of muse cell from human umbilical cord-derived for spinal cord injury in rats]. Zhongguo Gu Shang. 2019;32(4):327–34.
19. Guo Y, Xue Y, Wang P, Cui Z, Cao J, Liu S, et al. Muse cell spheroids have therapeutic effect on corneal scarring wound in mice and tree shrews. Sci Transl Med. 2020;12(562):eaaw1120.
20. Yamada Y, Wakao S, Kushida Y, Minatoguchi S, Mikami A, Higashi K, et al. S1P-S1PR2 axis mediates homing of muse cells into damaged heart for long-lasting tissue repair and functional recovery after acute myocardial infarction. Circ Res. 2018;122(8):1069–83.
21. Kadry H, Noorani B, Cucullo L. A blood-brain barrier overview on structure, function, impairment, and biomarkers of integrity. Fluids Barriers CNS. 2020;17(1):69.
22. Hermans EC, Donega V, Heijnen CJ, et al. CXCL10 is a crucial chemoattractant for efficient intranasal delivery of mesenchymal stem cells to the neonatal hypoxic-ischemic brain. Stem Cell Res Ther. 2024;15(1):134. Published 2024 May 7.
23. Takata F, Nakagawa S, Matsumoto J, Dohgu S. Blood-brain barrier dysfunction amplifies the development of neuroinflammation: Understanding of cellular events in brain microvascular endothelial cells for prevention and treatment of BBB dysfunction. Front Cell Neurosci. 2021;15:661838.
24. Daneman R, Prat A. The blood-brain barrier. Cold Spring Harb Perspect Biol. 2015;7(1):a020412.
25. Gray MT, Woulfe JM. Striatal blood-brain barrier permeability in Parkinson's disease. J Cereb Blood Flow Metab. 2015;35(5):747–50.
26. Nagatsu T, Mogi M, Ichinose H, Togari A. Changes in cytokines and neurotrophins in Parkinson's disease. J Neural Transm Suppl. 2000;(60):277 – 90. https://doi.org/10.1007/978-3-7091-6301-6_19. PMID: 11205147.
27. Esteves AR, Munoz-Pinto MF, Nunes-Costa D, Candeias E, Silva DF, Magalhaes JD, et al. Footprints of a microbial toxin from the gut Microbiome to mesencephalic mitochondria. Gut. 2023;72(1):73–89.
28. Bravo GA, Cedeno RR, Casadevall MP, Ramio-Torrenta L. Sphingosine-1-Phosphate (S1P) and S1P signaling pathway modulators, from current insights to future perspectives. Cells. 2022;11(13):2058.
29. Spiegel S, Milstien S. The outs and the Ins of sphingosine-1-phosphate in immunity. Nat Rev Immunol. 2011;11(6):403–15.
30. Prager B, Spampinato SF, Ransohoff RM. Sphingosine 1-phosphate signaling at the blood-brain barrier. Trends Mol Med. 2015;21(6):354–63.
31. Idriss HT, Naismith JH. TNF alpha and the TNF receptor superfamily: structure-function relationship(s). Microsc Res Tech. 2000;50(3):184–95.
32. Aggarwal BB, Gupta SC, Kim JH. Historical perspectives on tumor necrosis factor and its superfamily: 25 years later, a golden journey. Blood. 2012;119(3):651–65.
33. Xia P, Wang L, Gamble JR, Vadas MA. Activation of sphingosine kinase by tumor necrosis factor-alpha inhibits apoptosis in human endothelial cells. J Biol Chem. 1999;274(48):34499–505.
34. De Palma C, Meacci E, Perrotta C, Bruni P, Clementi E. Endothelial nitric oxide synthase activation by tumor necrosis factor alpha through neutral Sphingomyelinase 2, sphingosine kinase 1, and sphingosine 1 phosphate receptors: a novel pathway relevant to the pathophysiology of endothelium. Arterioscler Thromb Vasc Biol. 2006;26(1):99–105.
35. Hori E, Hayakawa Y, Hayashi T, Hori S, Okamoto S, Shibata T, et al. Mobilization of pluripotent multilineage-differentiating stress-enduring cells in ischemic stroke. J Stroke Cerebrovasc Dis. 2016;25(6):1473–81.
36. Healy LM, Antel JP. Sphingosine-1-phosphate receptors in the central nervous and immune systems. Curr Drug Targets. 2016;17(16):1841–50.
37. Garcia JG, Liu F, Verin AD, Birukova A, Dechert MA, Gerthoffer WT, et al. Sphingosine 1-phosphate promotes endothelial cell barrier integrity by Edg-dependent cytoskeletal rearrangement. J Clin Invest. 2001;108(5):689–701.
38. Camerer E, Regard JB, Cornelissen I, Srinivasan Y, Duong DN, Palmer D, et al. Sphingosine-1-phosphate in the plasma compartment regulates basal and inflammation-induced vascular leak in mice. J Clin Invest. 2009;119(7):1871–9.
39. Singleton PA, Dudek SM, Chiang ET, Garcia JG. Regulation of sphingosine 1-phosphate-induced endothelial cytoskeletal rearrangement and barrier enhancement by S1P1 receptor, PI3 kinase, Tiam1/Rac1, and alpha-actinin. FASEB J. 2005;19(12):1646–56.
40. Wojciak-Stothard B, Potempa S, Eichholtz T, Ridley AJ. Rho and Rac but not Cdc42 regulate endothelial cell permeability. J Cell Sci. 2001;114(Pt 7):1343–55.
41. Sanchez T, Skoura A, Wu MT, Casserly B, Harrington EO, Hla T. Induction of vascular permeability by the sphingosine-1-phosphate receptor-2 (S1P2R) and its downstream effectors ROCK and PTEN. Arterioscler Thromb Vasc Biol. 2007;27(6):1312–8.
42. Ogura F, Wakao S, Kuroda Y, Tsuchiyama K, Bagheri M, Heneidi S, et al. Human adipose tissue possesses a unique population of pluripotent stem cells with nontumorigenic and low telomerase activities: potential implications in regenerative medicine. Stem Cells Dev. 2014;23(7):717–28.
43. Uchida H, Morita T, Niizuma K, Kushida Y, Kuroda Y, Wakao S, et al. Transplantation of unique subpopulation of fibroblasts, muse cells, ameliorates experimental stroke possibly via robust neuronal differentiation. Stem Cells. 2016;34(1):160–73.
44. Suzuki T, Sato Y, Kushida Y, Tsuji M, Wakao S, Ueda K, et al. Intravenously delivered multilineage-differentiating stress enduring cells dampen excessive glutamate metabolism and microglial activation in experimental perinatal hypoxic ischemic encephalopathy. J Cereb Blood Flow Metab. 2021;41(7):1707–20.
45. Shimamura N, Kakuta K, Wang L, Naraoka M, Uchida H, Wakao S, et al. Neuroregeneration therapy using human muse cells is highly effective in a mouse intracerebral hemorrhage model. Exp Brain Res. 2017;235(2):565–72.
46. Abe T, Aburakawa D, Niizuma K, Iwabuchi N, Kajitani T, Wakao S, et al. Intravenously transplanted human multilineage-differentiating

stress-enduring cells afford brain repair in a mouse lacunar stroke model. Stroke. 2020;51(2):601–11.
47. Zhang YT, He KJ, Zhang JB, Ma QH, Wang F, Liu CF. Advances in intranasal application of stem cells in the treatment of central nervous system diseases. Stem Cell Res Ther. 2021;12(1):210.
48. Yamamoto S, Shiraishi K, Kushida Y, Oguma Y, Wakao S, Dezawa M, Kuroda S. Nose-to-brain delivery of human muse cells enhances structural and functional recovery in the murine ischemic stroke model. Sci Rep. 2025;15(1):16243.
49. Bovetti S, Hsieh YC, Bovolin P, Perroteau I, Kazunori T, Puche AC. Blood vessels form a scaffold for neuroblast migration in the adult olfactory bulb. J Neurosci. 2007;27(22):5976–80.

Publisher's note